SANDIA REPORT
SAND2009-6329
Unlimited Release
Printed September 2009

Electrostatic Microvalves Utilizing Conductive Nanoparticles for Improved Speed, Lower Power, and Higher Force Actuation

Christopher Apblett, Greg Ten Eyck, Eric Branson, Adam Cook, Andrew Collord, Rick Givler,

Josh Tice, Ben Schudel, Amit Desai, Paul J. A. Kenis

Prepared by Chris Apblett
Sandia National Laboratories
Albuquerque, New Mexico 87185 and Livermore, California 94550

Sandia is a multiprogram laboratory operated by Sandia Corporation,
a Lockheed Martin Company, for the United States Department of Energy's
National Nuclear Security Administration under Contract DE-AC04-94AL85000.

Issued by Sandia National Laboratories, operated for the United States Department of Energy by Sandia Corporation.

Available to DOE and DOE contractors from
U.S. Department of Energy
Office of Scientific and Technical Information
P.O. Box 62
Oak Ridge, TN 37831

Telephone: (865) 576-8401
Facsimile: (865) 576-5728
E-Mail: reports@adonis.osti.gov
Online ordering: http://www.osti.gov/bridge

Available to the public from
U.S. Department of Commerce
National Technical Information Service
5285 Port Royal Rd.
Springfield, VA 22161

Telephone: (800) 553-6847
Facsimile: (703) 605-6900
E-Mail: orders@ntis.fedworld.gov
Online order: http://www.ntis.gov/help/ordermethods.asp?loc=7-4-0#online

SAND 2009-6329
Unlimited Release
Printed September 2009

Electrostatic Microvalves Utilizing Conductive Nanoparticles for Improved Speed,

Lower Power, and Higher Force Actuation

Christopher Apblett
Ceramic Processing and Inorganic Materials
Sandia National Laboratories
PO Box 5800
Albuquerque, NM 87185-1349
Greg Ten Eyck
Microdevice Technologies
Rick Givler
Thermal and Fluid Processes
Eric Branson, Adam Cook, Andrew Collord
Ceramic Processing and Inorganic Materials

Josh Tice, Ben Schudel, Amit Desai, Paul J. A. Kenis
University of Illinois, Champaign Urbana

Abstract

We have designed and built electrostatically actuated microvalves compatible with integration into a PDMS based microfluidic system. The key innovation for electrostatic actuation was the incorporation of carbon nanotubes into the PDMS valve membrane, allowing for electrostatic charging of the PDMS layer and subsequent discharging, while still allowing for significant distention of the valveseat for low voltage control of the system. Nanoparticles were applied to semi-cured PDMS using a stamp transfer method, and then cured fully to make the valve seats. DC actuation in air of these valves yielded operational voltages as low as 15V, by using a supporting structure above the valve seat that allowed sufficient restoring forces to be applied while not enhancing actuation forces to raise the valve actuation potential. Both actuate to open and actuate to close valves have been demonstrated, and integrated into a microfluidic platform, and demonstrated fluidic control using electrostatic valves.

Table of Contents

Table of Figures

Background

Microfluidic systems hold the promise to dramatically improve the rate and depth of development for biological discovery and control. As such, medical applications and homeland security, specifically for detection of potentially hazardous biowarfare agents drive the need for far more space and energy efficient micro-fluidic systems with increased complexity. Of all of the subcomponents within a microfluidic system, the valve is the most difficult to realize. Yet valves are the components which control both how fluids move through the system, as well as control which fluids are allowed to interact, which are at the most basic function of all microfluidic systems. Current valve systems are based largely on flexible membranes that are deflected into a microchannel to block flow[1],[2], although others based on bubble nucleation within the fluid[3] and changes in rheology have also been demonstrated or proposed. The Quake team at Berkeley has developed perhaps the most well established valve system, comprised of two crossing fluidic channels separated by a thin membrane in the simplest case. When the upper "control layer" channel is pressurized, the membrane is distended into the lower "fluidic" channel, effectively blocking flow of fluids within this channel. Other methods to blocking of water channel have also produced useful devices; however, they have all suffered limitations to adoption because of the relatively large energy input needed or significant functional overhead (in the form of off-chip pressure generators) necessary to realize their function.

The advent of large scale integration in microfluidic systems has enabled multi-step, high-throughput, and massively parallel operations to be performed on a single chip with applications diverse as the synthesis of radiolabeled imaging probes[4] and gene expression screening.[5] A pneumatic microvalve was one of the key technological innovations that made these early successes possible.[6] This microvalve has been widely adopted in the field mainly due to the

simple fabrication with soft lithographic techniques and straight-forward monolithic incorporation into microfluidic devices. Unfortunately, pneumatic microvalves require ancillaries including a pressurized gas source, an array of solenoid valves, and computerized controls to operate the device, which severely limits portability. Other valve technologies, e.g. magnetic, thermal, or electrochemical, have also been developed,[7] but none of these have been incorporated into highly integrated microfluidic networks mainly due to intensive microfabrication or lack of versatility.

Electrostatic valves represent the lowest energy option currently, with only very short timescales for charge and discharge (during which time charge is either added or removed from the actuation plates). In steady state (either actuated or open), no power is consumed. However, electrostatic valves suffered from having relatively limited displacements, and had limited displacements due to the concern that excessive displacements would permanently distend or damage either the valve membrane, the actuating electrode, or both. In light of this challenge, we proposed to develop a new valve that can be monolithically integrated with existing microfluidic systems but will actuate electrically rather than pneumatically. This innovation would allow for a massive reduction in power and ancillary hardware necessary for microfluidic systems, while increasing the speed of valve actuation and the pressure isolation capability of the valves. This new valve represented a combination of the ease of integration of an electrostatic valve with the performance of a pneumatic valve. The footprint needed per valve would be decreased (since no crossing pneumatic actuation channel would be necessary); these valves could also be constructed such that they are closed in the rest state (actuate-to-open concept), as is desired for most applications. Such a change in actuation will require new understanding and new science to correctly exploit the physics of the new valve, as these valves will have electric

fields and electrical conductors that are severely deformed, taking them outside of the realm of traditional valve behavior.

To achieve maximum flexibility with maximum distension of the valve seat, we chose to incorporate conductive nanotubes into a polymeric membrane. This configuration allowed for the membrane to be significantly deformed, but have little impact on the conductive path formed by the nanoparticles. The key technical hurdle in this path was to incorporate conductive nanoparticles into the thin flexible membranes that comprise the microvalve seat so that the membranes become electrically conductive. They must also maintain this electrical conductivity through their range of deflection. Because of this, it was thought necessary to be able to pattern the electrostatic valve itself as well as the electrical connection to the valve in a method compatible with existing microfluidic chip assembly. We were also interested in developing a simple process that could, eventually, be transferred to a roll-to-roll process to allow for low cost mass manufacture of the microfluidic systems. Wherever possible, simple processes, such as casting over forms and stamping, were used to make this scale up process as easy as possible.

We have developed an electrostatically actuated microvalve which retains the versatility of pneumatic valves while reducing the bulk of ancillaries needed for operation. While many electrostatic precedents have been reported,[7,8,9] we fabricated microvalves exclusively with soft lithographic techniques, using nanoparticles to confer conductivity to the required elements. Consequently, the incorporation of these microvalves into microfluidic integrated networks should be as straight-forward as their pneumatic predecessor. We report the development of an analytical model to guide the design of electrostatic microvalves, several methods which were investigated for embedding nanoparticles in elastomeric films, and the subsequent fabrication and initial tests of arrays of microvalves.

Analytical Model

Motivation for an analytical model to describe operation of electrostatic valves

The operation of electrostatic valves in microfluidics involves several physical phenomena, such as coupling between mechanical deformation and electric fields, static and dynamic motion in viscous and pressurized fluids, and adhesion driven collapse of flexible membranes. The simultaneous existence of these phenomena necessitates a systematic model to describe the operation of the valve and guide the design process in order to ensure low actuation potential within the limits of valve integration capabilities in complex microfluidic chips. Additionally, the analytical model will enable better interpretation of the experimental results and reduce subsequent iterations in the design process.

We extend the analytical models in literature to microfluidic applications by considering several issues conventionally ignored in electrostatic actuation of microscale structures, such as multi-layer components, material properties of polydimethylsiloxane (PDMS), collapse of valves, and actuation in liquids. The analytical model is used to explicitly identify the critical design parameters and to provide a set of design rules or guidelines for optimal valve operation by minimizing the actuation potentials. Although the model is discussed with respect to microfluidic valves, it is applicable to various other applications, such as pneumatic actuation of valves and microfluidic pumps.

Description of the analytical model and governing equations

The electrostatic valve is modeled as a thin flat membrane that is clamped at the outer edges (Figure 1). The membrane is coated with a conducting material, forming the top electrode, and is suspended over a fixed conducting plate, which forms the bottom electrode (separated by a distance g). The two electrodes function as two plates of a parallel plate capacitor, where one

plate is movable and attached to a spring of spring constant *k*. An applied potential creates an electric field between the plates, which in turn causes the electrostatic forces to pull the movable plate (deflect the membrane) towards the fixed plate. The deflected profile of the membrane is shown in Figure 1, which will cause the valve to impede flow in the channel. In Figure 1, *V* is the applied potential and *y* is the displacement of the movable electrode or membrane. Note that *y* is also the deflection of the spring and *g* is the height of the microfluidic channel.

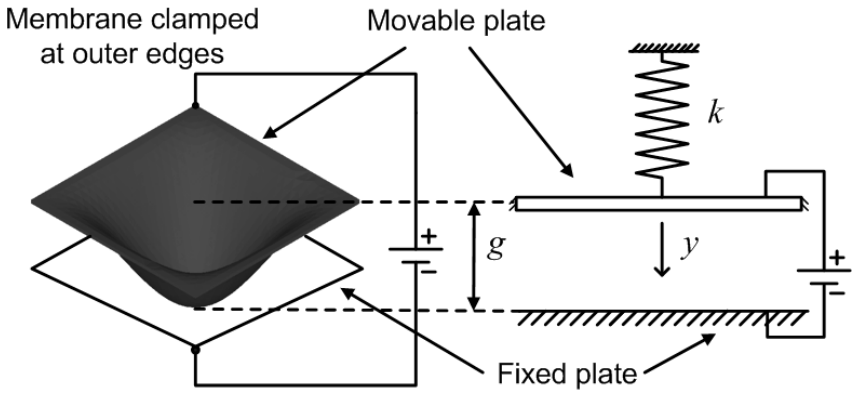

Figure 1: Parallel plate capacitor model for the electrostatic valve.

The expression for static stiffness (*k*) of a square or circular membrane (the two most common geometries for microfluidic valves) that is fixed or clamped along the outer edges under a uniformly distributed load is given by equation A1 in the appendix. The expression is derived from standard membrane deflection equations, and various factors are included to account for aspect ratio (K_{AR}), bilayer configuration (relatively stiff conducting layer on valve membrane, $K_{bilayer}$) and membrane stresses due to large deflections (K_{MS}). Note that $K_{bilayer}$, K_{AR} and K_{MS} are typically ignored in analysis of electrostatic valves, which can lead to significant differences in analytical predictions and actual valve operation. The expression for stiffness represents the stiffness per unit area, since the mechanical loading due to electrostatic fields is distributed over

the entire membrane. If p is the uniform lateral pressure acting on the membrane and y_{max} is the lateral deflection of the center of the membrane, then $p = ky_{max}$.

The electrostatic actuation of the valve is described in terms of motion of a parallel plate capacitor, with one plate fixed and the other attached to a linear spring. In case of deflection of a membrane (or any deformable structure) due to forces produced by an electric field between parallel plates, a point of instability (critical deflection) exists until which point the electrostatic forces and the restoring mechanical forces are in equilibrium.[10] Beyond the point of instability, the membrane collapses or snaps in, and this snap-in is known as pull-in instability. The critical deflection is given by

$$y_{snapin} = \frac{1}{3}\left(h_c \frac{\varepsilon_{fluid}}{\varepsilon_m} + g \right), \qquad (1)$$

where ε_{fluid} and ε_m are the relative permittivity of the fluid and membrane material, respectively, and h_c is the distance between the conducting layer and bottom of the membrane. If $y_{snapin} > g$, the electrostatic valve is in the stable deflection region and the actuation potential required to close the valve is given by

$$V_{close} = \sqrt{\frac{2kg\left(h_c \frac{\varepsilon_{fluid}}{\varepsilon_m} \right)^2}{\varepsilon_0 \varepsilon_{flluid}}}, \qquad (2)$$

where ε_0 is permittivity of free space. If $y_{snapin} \leq g$, the actuation of the valve is governed by pull-in instability and the potential required to close the valve is given by

$$V_{close} = \sqrt{\frac{8k\left(g + \left(h_c \frac{\varepsilon_{fluid}}{\varepsilon_m} \right) \right)^3}{27\varepsilon_0 \varepsilon_{fluid}}}. \qquad (3)$$

Validity of the analytical model for different scenarios in microfluidic applications

Dynamic operation of the valves: Although the expressions for membrane stiffness are derived for static operation of valves, the expressions are valid as long as the operating frequencies of the valve are lower than the natural frequency of the membrane, i.e. the inertial effects of the membrane can be neglected. For typical PDMS membranes, the natural frequency (15 KHz) is much higher than the operating frequencies in dynamic applications (e.g. 100 Hz in peristaltic pumps).

Fluids with high viscosity: One of the main mechanisms to describe the influence of fluid viscosity is squeeze film damping, which accounts for the energy dissipation due to expansion and compression of viscous fluids between a fixed and vibrating flat plate. The squeeze film damping results in an additional stiffness term given by $k_{fluid} = \left(96\mu L_e^{\,2}\omega\right)/\left(\pi^4 g\right)$, where ω is the vibration frequency of the membrane and L_e is the equivalent planar dimension of the membrane.

Pressurized fluids: The electric field produced between the membrane and the fixed electrode will have to perform work against the flow pressure (p_{flow}), which results in an increase in actuation potentials (V_{flow}) given by

$$V_{flow} = \sqrt{\frac{2p_{flow}\left(g + t_m\left(\varepsilon_{fluid}/\varepsilon_m\right)^2\right)}{\varepsilon_0\varepsilon_{fluid}}}, \qquad (4)$$

where t_m is the thickness of the membrane.

Actuation in conducting fluids: In case of conducting liquids, such as water, the electric field results in formation of an electric double layer (EDL) that effectively shields the applied potential. To avoid the formation of EDL, an alternating or AC potential is applied to actuate the valve, and the frequency of the AC potential (f_{AC}) depends on geometry of the valve and

conductivity of the liquid. In such cases, if the mechanical response of the valve at frequency $2f_{AC}$ is negligible compared to the response at valve resonance frequency ($f_{resonance}$), i.e. $2f_{AC} > f_{resonance}$, then the actuation potential V_{close} will be the root mean square (rms) value of the applied AC potential (V_{rms}). For a typical valve made out of PDMS, the resonant frequency is 15 KHz, which is lower than twice the actuation frequency ($2f_{AC}$) for most fluids.[11]

Application of the analytical model to the design process

The governing equations of the analytical model can be used to identify critical design parameters that influence the actuation potential. Some obvious conclusions can be drawn from the equations, e.g. the membrane thickness is the most critical parameter that influences the potential. However, the equations also indicate that increasing the dielectric constant of the fluid will not necessarily decrease the actuation potential, which is contrary to inferences from conventional analysis of electrostatic actuation in liquids. The reason for this counter-intuitive observation is that the thickness of the membrane, which is traditionally ignored, is comparable to the channel height.

The analytical model can estimate the design parameter space subject to constraints on the actuation potentials. For example, Figure 2 shows the design parameter space with respect to aspect ratio (*D/tm*) and relative thickness (*g/tm*) ratio, for a 500 μm diameter (*D*) membrane actuated in air for actuation potentials less than 50 V. The geometrical parameters for the valve are chosen such that the valve dimensions are within the limits of the fabrication processes. Figure 2 is a contour plot of actuation potentials, with a contour spacing of 1 V and the potential values decreasing from 50 V to 15 V towards the top left direction. The region with contour lines represents the parameter values for actuation potentials lower than 50 V. Thus, the analytical model is useful to estimate the range of actuation potentials subject to constraints on

valve dimensions, which in turn are determined by fabrication limitations and functional requirements.

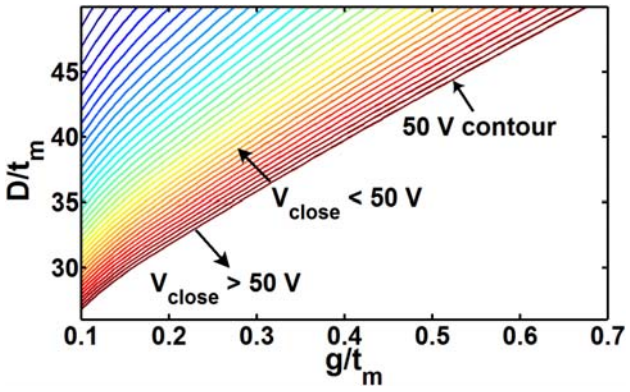

Figure 2: Design parameter space for potentials less than 50 V.

Another important observation deduced from the analytical model is the significant influence of residual stresses on the electrostatic valve operation. The fabrication of freestanding membranes results in residual stresses, and the effect of residual stresses is significant when σ0 (residual stress) is comparable to Em(tm/Le)2. With respect to the design parameter space, the influence of residual stresses is to shrink the space and place more restrictions on the geometry of the valve. For example, the design parameter space for different residual stresses is shown in Figure 3, which is a contour plot with the contour lines corresponding to actuation potentials of 50 V. The set of parameter values to the upper left of the contour lines correspond to actuation potentials lower than 50 V.

The residual stresses in PDMS membranes, freestanding and on substrate, have been measured to be approximately 0.1 – 0.15 MPa,[12,13] which implies that the residual stresses significantly influence the actuation potentials.

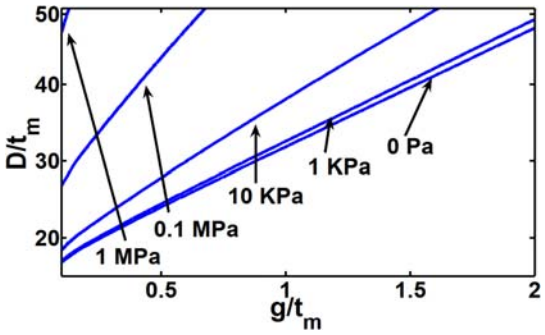

Figure 3: Effect of residual stresses on design parameter space. The lines correspond to 50 V contour lines.

An important design consideration for electrostatic valves (and valves in general) is collapse of the valve onto the floor of the channel. The collapse can occur either during assembly of the microfluidic chip (self-collapse) or the valves remain stuck to the floor even after the actuation potential is removed (pressure-driven collapse). This collapse of valves is primarily driven by interfacial adhesion between the valve membrane and floor of the channel, and is especially significant in microfluidic chips made out of soft polymers (e.g. PDMS) due to the high adhesion energies of the polymers. The collapse of free-standing structures due to interfacial adhesion has been analytically modeled in case of micromachined silicon-based structures or MEMS, and is commonly referred to as 'stiction'.[14] Based on the models, we define a dimensionless parameter (Ψ) that determines whether the valves collapse or not during the actuation, and is given by

$$\Psi \approx \eta_1 \frac{\gamma L_e^{\,4} K_{AR}}{E_{bm} t_m^{\,3} g^{\,2} K_{bilayer}} \left[1 + \eta_2 \frac{\sigma_0}{E_{bm}} \left(\frac{L_e}{t_m} \right)^2 + \eta_3 \left(\frac{g}{t_m} \right)^2 \right]^{-1}, \quad (5)$$

where γ is the interfacial adhesion energy, and η_1, η_2, and η_3 are constants dependent on membrane shape and boundary conditions . A critical value for Ψ exists ($\Psi_{critical} = 1$) , and Ψ values greater than the critical value will result in valve collapse due to adhesion. From equation 5, we can infer that any effort to minimize Ψ (e.g. stiffening of the membrane) will increase the

actuation potential, and hence it is desired to operate around $\Psi_{critical}$ to ensure low actuation potentials and no collapse of valves.

Design rules or guidelines based on the analytical model

The design rules for electrostatic valves can be broadly classified into two categories, mechanical and electrical design rules.

Mechanical design rules

1. Analytical modeling shows that low stiffness values for the valve membranes are possible to achieve within the limits of the fabrication processes for PDMS valves in microfluidics, which will result in low actuation potentials.
2. Equations (1) and (2) estimate the actuation potential for the valves based on the valve geometry and material properties of the valve and fluid.
3. Residual stresses in the valve membrane significantly influence the overall stiffness, especially if the membrane is thin and made of polymeric materials with low Young's modulus. Strategies for reducing residual stresses, such as room temperature curing and multilayer membranes, are critical towards achieving low actuation potentials.
4. To prevent collapse of valves due to adhesion and to ensure low actuation potentials, the material and geometrical parameters need to be adjusted to operate around $\Psi_{critical}$.

Electrical design rules

1. Pull-in operation (snap-in) is desirable because in that case, actuation potential needs to be only large enough to deflect the valve membrane until the point of the critical deflection. As a result, the energy requirement for the valve operation is reduced as opposed to the case of stable valve deflection. The geometrical parameters of the

valve and, to some extent, the relative permittivity of the membrane material can be adjusted to significantly lower the point of instability.

2. Uniformity of the conducting film influences the final actuation potentials, due to the cracks in the film acting as micro-dielectric domains. A technique to minimize the effect of discontinuous films is to introduce compressive stresses in the films, which will tend to close up the cracks.
3. Strategies to reduce the effect of parasitic charging at the membrane-fluid interfaces, such as reversal of polarity of the electrodes after every actuation, will result in lower actuation potentials.[15]

Miscellaneous applications of the model

Although the analytical model was derived for static deflection of valves in non-viscous fluid flow, it can be adapted to various applications of electrostatic actuation.

1) During dynamic actuation of the valves for peristaltic pumps in microfluidics, the inertial effects of PDMS microvalves can be ignored and the equations for static membrane stiffness are valid.
2) The viscosity of the fluid becomes important during dynamic actuation in liquids. The squeeze film damping mechanism results in additional viscous forces on the valve membrane.
3) An alternating potential (V_{rms}) is applied in case of electrostatic actuation in conducting fluids to minimize the formation of electric double layer. In that case, V_{rms} can be estimated using standard equations for actuation potential for PDMS based microvalves.

4) The effect of fluid pressure in high-pressurized flow leads to increase in actuation potentials.

Conducting elastomeric membranes

As reflected in the model, the central component of our microvalve design was a flexible, conducting, elastomeric membrane. Before fabricating the full microvalve assembly, we investigated several methods for embedding conducting nanoparticles into the membrane, enabling large deflections without a loss of conductivity. In all, we explored three different approaches: i) directly mixing the nanoparticles into the elastomer precursors prior to processing, ii) airbrushing nanoparticles onto a pre-existing membrane, and iii) forming a film of nanoparticles by filtration and subsequently transferring the film to the membrane via microtransfer printing.

Directly mixing nanoparticles into elastomer precursors

We initially attempted embedding nanoparticles in uncured PDMS and then processing the slurry into a thin membrane suitable for deflection. Some precedents were found in the literature, though mainly for the creation of elastomeric electrical sensors rather than actuators.[16] Liu et al. embedded multi-walled carbon nanotubes (MWNT) into PMDS precursors and then used the slurry to fill the gaps of a mold of photoresist. Residual slurry was removed with a razor blade, and after curing, the photoresist was removed with a suitable solvent.[17] By using this "doctor-blading" technique, the researchers were able to pattern micron-sized structures of the conducting elastomer. The researchers also found that MWNT possessed a favorable percolation threshold compared with spherical conducting nanoparticles such as carbon black.[17] Consequently, for most of the initial studies reported here, MWNT were used as the conducting material in our membranes.

We adopted Liu's approach and patterned photoresist around large rectangular regions on a silicon wafer, filled the recess with a MWNT/PDMS slurry (usually 10 wt% MWNT), and then slid a razor blade across the rectangular region, using the photoresist to effectively define the height of the MWNT/PDMS membrane. While the resulting membranes were conductive, we encountered several difficulties. Firstly, streaking caused non-uniformities in membranes. This may have been due to the size of the nanoparticles (the MWNT we used were as long as 10 μm), the roughness of the razor blade, or the speed at which the blade was drawn across the mold. Secondly, the thickness of the membranes was difficult to control, perhaps due to uneven pressure applied by the researcher. Lastly, we believe the concentration of nanoparticles in the slurry increased the stiffness of the membrane, and estimates from our model predicted that we would need membranes significantly thinner than we were able to fabricate. It should also be noted that we tried compressing the MWNT/PDMS slurry instead of doctor-blading, but in this process, the MWNT tended to clump together and prevent thin, smooth films from forming.

Airbrushing

We next attempted airbrushing a solution of MWNT directly onto a PDMS membrane. Conductive MWNT films have been airbrushed onto various surfaces such as glass and plastics for photovoltaic applications.[18] The films can be made thin enough to be transparent, in contrast to the doctor-blading approach where membranes were opaque. MWNT were suspended in an aqueous solution with the aid of a surfactant, sodium dodecyl sulfate (SDS), and separately, PDMS was spin-coated onto a silicon wafer and fully cured. Afterward, the aqueous solution of MWNT and SDS was airbrushed as evenly as possible onto the surface. After a certain threshold coverage was achieved, the films conducted, and if properly masked, we imagine that the films could be patterned. We also encountered difficulties with this approach, however. When

observed under the microscope, the films had noticeable surface heterogeneities. Literature suggests that this is due to the rate of evaporation from the aerosols emitted from the airbrush.[19] If the solvent evaporates too quickly before the solution reaches the substrate, then the MWNT aggregate before being deposited. Alternatively, if the solution does not adequately evaporate, then liquid drops form on the surface of the substrate, and this deposits MWNT unevenly. In the course of the experiments, this latter phenomenon was observed when the airbrush was held too close to the substrate or if the rate of flow was too heavy. Secondly, if the surfactant were not removed from the deposited film, encapsulating layers of PDMS would not adhere to the MWNT film, and the membrane would delaminate.

Filtration and microtransfer printing

Both doctor-blading and air-brushing failed to yield conducting membranes that were uniform, either in terms of thickness or uniformity of nanoparticles distribution. Filtration of a MWNT suspension, however, was previously shown to yield highly uniform, conductive, and transparent films.[19] MWNT were suspended in an aqueous solution, again with the addition of SDS. The solution was sonicated to break up MWNT aggregates and subsequently centrifuged to isolate any bundles that could not be disintegrated. The solution was then filtered through a membrane, typically with a pore size of 0.2 μm. A uniform black film was formed on the filter resulting in a soapy, clear and colorless filtrate. After the solution was completely filtered, the film was washed with alcohol (isopropyl alcohol, methanol, or ethanol) until the filtrate was free of any bubbles. After drying, the MWNT film could be transferred directly to a pre-formed PDMS membrane.

Several filter materials were investigated for suitability for transferring MWNT films. Teflon® filters released MWNT films relatively easily; however, Teflon® filters with small pore

sizes were delicate and were manufactured with a polyethylene support mesh on the underside. This mesh produced a texture in the MWNT film, and in extremely thin films, the mesh caused discontinuities. Nylon, cellulose, polycarbonate, and polyester filter membranes were also investigated. However, none of these materials transferred MWNT films reliably, unless the film was thick (non-transparent). Usually, the top layers of the MWNT film would transfer, leaving a textured residual film behind. Filter membranes that consistently yielded the best results were composed of alumina (Whatman Anopore inorganic membranes). MWNT films could be completely transferred, even if very thin, leaving behind hardly any visible residue. It should be noted, however, that the inorganic membranes were brittle and had to be handled more carefully than the polymeric membrane filters.

We performed several characterization studies of conducting PDMS membranes fabricated in the above manner. Firstly, we quantified the dependence of resistivity on MWNT loading with no strain applied to the membrane (Figure 4a). Resistivity decreased and converged to a value of ~1 Ohm-cm as MWNT loading increased. Next, we applied a slow, periodic strain (60%, 2 hrs/cycle) to the membrane and observed the change in resistance (Figure 4b). The resistance increased as strain increased, but remained conductive until rupture. We did not observe any mechanical or electrical hysteresis during the stretch tests. We also applied rapid strains to the membrane and observed that after initially increasing, the resistance undergoes a transient reduction proportional to the induced strain and then levels off (Figure 4c). We assume that this behavior is due to the reorientation of the MWNT in the polymer after a rapid deformation. Overall, the performance characteristics of the conducting membrane proved amenable for its adaptation into an electrostatic microvalve. We can tune nanoparticles loading to control the conductivity of the film; the film retains conductivity over large deflections; and there is little

observable mechanical or electrical hysteresis due to deformation. Transparent films should be beneficial for visualizing fluid flow through microvalves or detecting analytes.

After finding a suitable means of conferring conductivity to elastomeric membranes, the next challenge was to develop a way to pattern the conducting areas in the membranes. Microcontact printing proved to be an easy yet highly effective solution.[20] After MWNT were filtered to form a thin film, a patterned PDMS stamp (20 PDMS monomer: 1 PDMS cross-linker weight ratio, hereafter referred to as 20:1 PDMS) was brought into conformal contact with the film, slight pressure was applied by hand, and then the stamp was removed along with the selected areas of the film. When the stamp was pressed onto a PDMS membrane, the MWNT were released onto the new substrate. For the transfer to happen reliably, the PDMS membrane was also made of 20:1 PDMS, although it was not cured to the same degree, ensuring that the receiving surface was tackier than the stamp. Membranes or slabs of PDMS with different weight ratios of cross-linker were also capable of receiving the MWNT film from the PDMS stamp, but again, the substrates were under-cured so that they were tackier than the stamp. If the receiving PDMS membrane was too tacky, the stamp and membrane tended to adhere too strongly to be separated. We were able to create patterns as small as 50 μm wide, although we believe smaller features are possible.

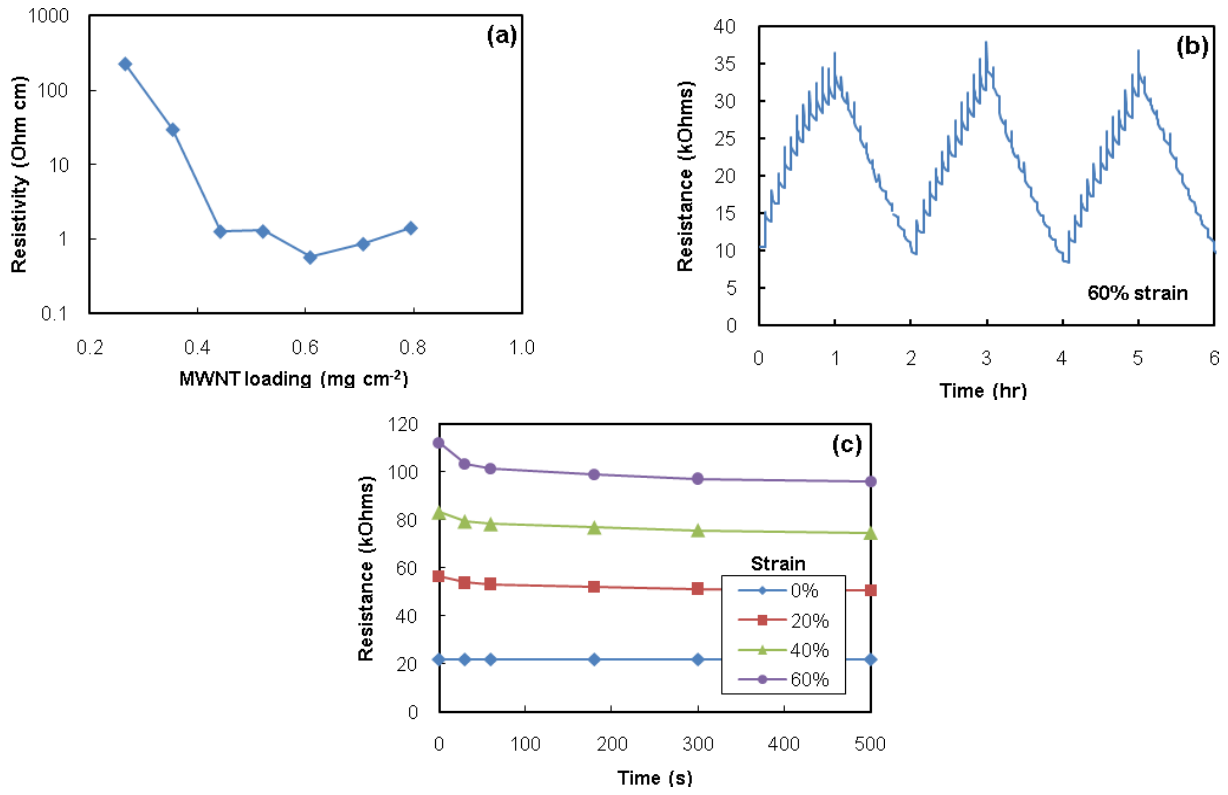

Figure 4: Characterization of conducting membranes made by directly transferring MWNT films from filters to PDMS membranes. (a) Dependence of resistivity on MWNT loading. (b) Graph showing no detectable electrical hysteresis after slow stretching and relaxation. (c) Loss in resistance after rapid stretching.

Wet vs. Dry Nanotube Encapsulation

Another option explored for the electrostatic valve this summer was the decoupling of the electrostatic actuation from the flow of fluid. In this setup, a dry, electrostatic portion of a control layer would compress under voltage, which in turn would force valves to collapse in a wet, fluid controlled area on the chip.

While this device appeared promising, current fabrication techniques of the nanotube electrodes led to some problems preventing valve operation <50 volts. Dry versus wet encapsulation of multi-walled carbon nanotubes (MWCTs) were both compared as an incorporation technique within the device assembly. These techniques focus on how best to compose the two patterned nanotube layers such that only low voltage is necessary for the valves to collapse. Dry encapsulation involves stamping the nanotubes directly onto a cured PMDS layer with a crosslinker ratio of 15:1. To encapsulate this layer, another cured layer with a crosslinker ratio of 5:1 is aligned over these nanotubes (Figure 5). In the areas where these layers contact, the different in crosslinker ratio is enough to create a permanent seal after heating at 70 C for 1 hour as demonstrated by Quake et al.[21] One advantage for this process is the reduction of encapsulation layers within the device, which brings the nanotube layers in closer proximity, thus reducing required voltage by a square root value.

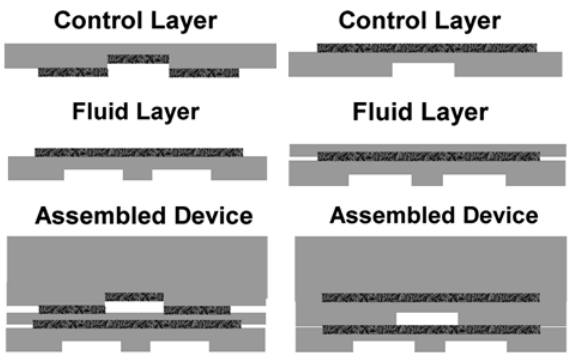

Figure 5: Device assembly for dry encapsulation (left) and wet encapsulation (right) for assembly of PDMS-based microvalves using multilayer soft lithography.

In wet encapsulation, both MWCT layers are patterned directly onto a hard PDMS layer, but then coated in place with a liquid PDMS layer spun directly onto the patterned nanotubes. Device assembly still follows the assembly of a 15:1 layer to a 5:1 layer, but the nanotubes themselves are encapsulated into wet PDMS that cures around the patterned nanotube structures. An advantage to this process is that the nanotubes are forced into a flat layer, since the wet PDMS manages to fill in

The fabrication process for stamping these tubes inside of the device is important, because for each layer that is added between the nanotube sheet, the required voltage actuation goes up exponentially. For these devices, MWCTs were patterned within control channels (Figure 5, left), as opposed to encapsulating devices within layers of wet PDMS (Figure 5, right). This was done primarily to reduce the amount of space between relevant layers in PDMS to achieve lower voltage requirements for valve actuation.

However, bringing the tubes in closer contact required reducing the layers of PDMS-based support layers in between. In so doing, the nanotubes were free to aggregate within the microfluidic channels, since they were not encased in wet PDMS on either side. Without a flat PDMS support structure that encapsulated the tubes before curing, the nanotubes created dusty particles within the chambers that did not adhere to a single side of the chamber. Rather than collapse, these devices would not actuate at any voltage (<500V). It is possible that during the steps of fabrication, the tubes themselves would prevent the layer from properly sealing (see Figure 6), causing very large (>100μm) gaps.

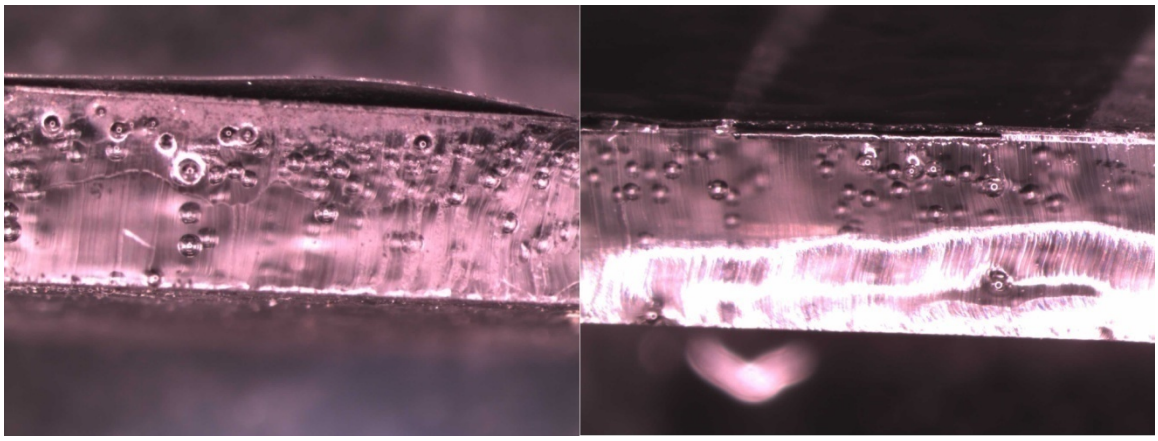

Figure 6 Left: A PDMS multilayer device that included a dry encapsulation of nanotubes placed between two cured PDMS layers. The layers have delaminated, due to the dry nanotubes preventing bonding between the PDMS layers. Right: A PDMS multilayer device including wet encapsulation of nanotubes, with a subsequent post-baking step. Both layers were measured for conductivity, (210 kΩ / cm dry, 180 kΩ / cm wet).

When these tubes were encapsulated within a wet PDMS layer, unsteady voltage actuation was seen at ~250V range. Dry encapsulation did not have an actuation. When the valves were cut open to observe how the patterned MWCTs change during wet or dry encapsulation (**Error! Reference source not found.**), it became apparent that the dry encapsulation process did not fix nanotubes in place. Within the individual valve compartments, the nanotubes were allowed to freely aggregrate, leading to no actuation potential. Since the nanotubes were not fixed during dry encapsulation, any voltage applied to these valves would merely move nanotubes around, instead of deform the layers to close shut.

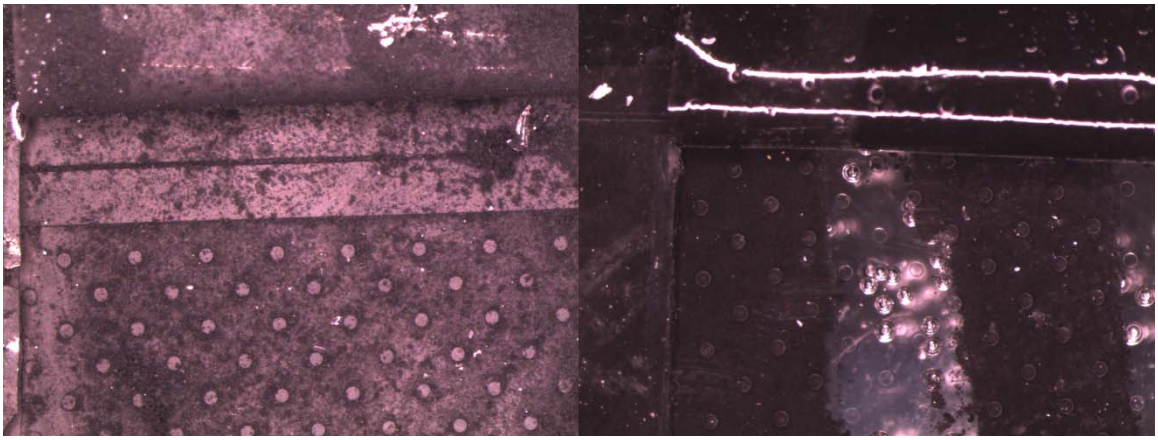

Figure 7 Left: A sliced portion of a PDMS device with nanotubes dry deposited onto the inside of a control layer. The nanotubes within the device have clustered mainly around the round posts within the chamber. Right: A sliced portion of a PDMS device with nanotubes imbedded beneath the control layer into a solid layer. These tubes do not aggregate, as they are encapsulated into wet PDMS before curing.

Even though wet encapsulation might create further insulation and increase voltage required to actuate, this function is necessary in order to ensure nanotubes remain in position as patterned rather than free to diffuse and aggregate within the valves.

Arrays of electrostatic microvalves

Fabrication

The fabrication of the electrostatic microvalve using the conducting elastomeric membranes may be summarized as follows (Figure 8). A thin film of MWNT was formed by vacuum filtration of an aqueous mixture of MWNT and SDS through a membrane, as discussed earlier. Separately, PDMS was spin-coated onto a mold to form channels and membranes. The MWNT film was subsequently transferred with a PDMS stamp onto the PDMS membrane. Electrical contacts were formed with a slurry of PDMS and MWNT, and after the contacts vulcanized, a second layer of PDMS was spin-coated on the previous layer to encapsulate the MWNT film. A slab of PDMS (hereafter referred to as the support layer) was sealed to the top-side of the membrane. The support layer contained open compartments above the actuating regions, often with the addition of support structures (e.g. posts) to prevent membranes from prematurely collapsing. After the layers fully cured together, the valve was removed from the mold and placed onto a lower electrode. For initial tests, the lower electrode consisted of a thin indium tin oxide (ITO) film evaporated onto a glass slide. The upper portions of the valve were not permanently sealed to the lower electrode so that the lower electrode could be reused. For tests with fluids in the channels, the upper layers were permanently sealed to a lower electrode made of PDMS and MWNT. To make the lower electrode, electrical contacts made with a MWNT/PDMS slurry were first laid onto a substrate, and PDMS was poured on top to make a relatively thick slab. Before the slab was fully cured, it was removed from the substrate and a MWNT film was patterned onto the underside via microtransfer printing. After, the MWNT side of the slab was pressed back onto a substrate, and the slab was allowed to fully cure. The top and bottom PDMS sections of the valve were sealed together with oxygen plasma after access

holes were drilled in the upper portion. A detailed process flow with specific parameters is included in Appendix B.

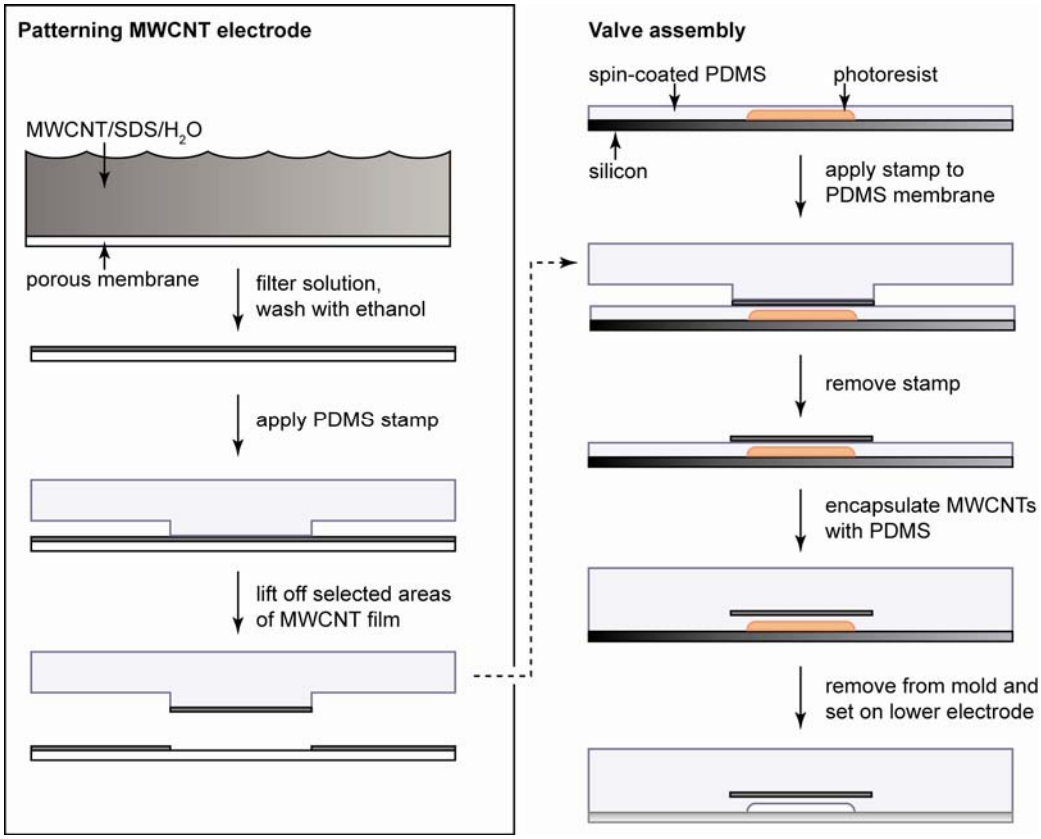

Figure 8: Process flow for fabricating electrostatic microvalves.

Actuation of arrays of electrostatic microvalves

We fabricated an array of microvalves with diameters ranging from 200-1000 µm and a constant channel height of 2 µm. Images obtained with scanning electron microscopy revealed that the PDMS membrane was 50 µm thick, with 10 µm of PDMS between the top of the channel and the MWNT film (Figure 9). (Unless otherwise noted, these dimensions are the same for all the valves discussed).

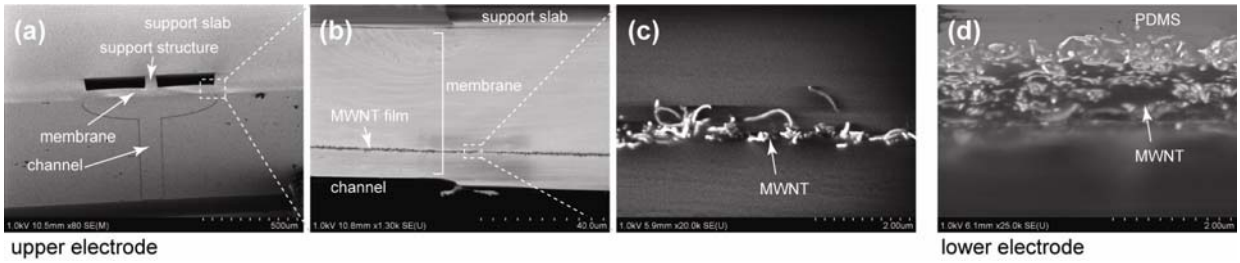

Figure 9: Scanning electron micrographs of cross-sections of electrostatic microvalves.

Several different geometries were tested for the support structures above the conducting membrane, including posts, spirals, and triangular beams. We initially performed tests by applying a potential between the conducting membrane and a lower electrode made from an ITO film on glass. Figure 10a shows an example of a set of valves that closed within milliseconds upon application of a 55 V potential. In close agreement with the model, valves with small diameters required a high potential to actuate, but as diameter increased, the actuation potential converged asymptotically to value of ~50 V for the design parameters presented here (Figure 10b). There are currently not enough data to clearly distinguish the effects of different support structure geometries, and the data shown in Figure 10b represent the results from valves with several different support structures. A more systematic investigation of the effect of support structures is presented next.

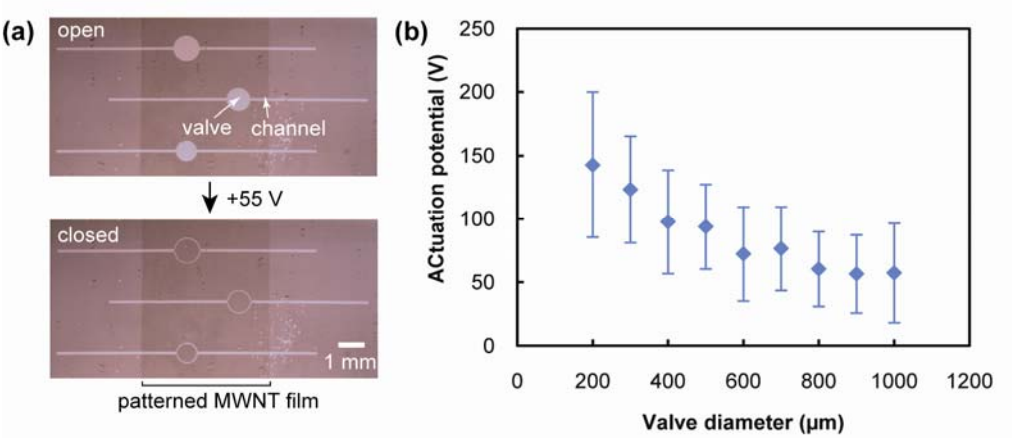

Figure 10: Electrostatic valve actuation on ITO/glass lower electrode. (a) Micrographs of valves before and after closure. (b) Actuation potentials needed to close valves of different diameters.

Effect of support structures on actuation potential

To systematically investigate the effect of support structures on actuation potential, we fabricated a series of valves with support posts of different diameter. The posts ranged from 50-100% the diameter of the valves. All of the posts were 50 μm tall. Figure 11 shows that as the post size decreased, so did the actuation potential needed to close the valve.

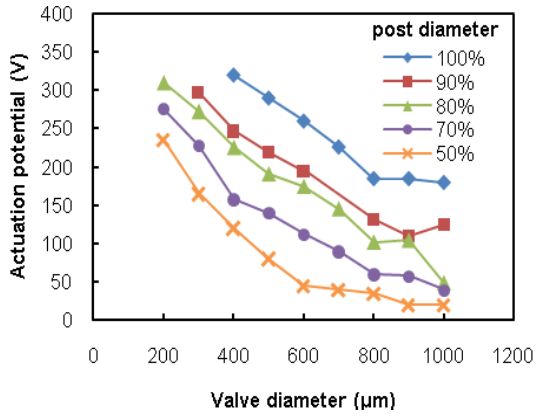

Figure 11: Actuation potentials for microvalves with membranes supported with PDMS posts. Percentages refer to the ratio of the post diameter to the diameter of the valve.

We found that the stiffness of the support structures also affected actuation potentials. A series of valves was made with solid slabs of PDMS used as the support system. We used different ratios of cross-linking agent to monomer in the support layers and found, predictably, that less cross-linked layers led to lower actuation potentials (Figure 12).

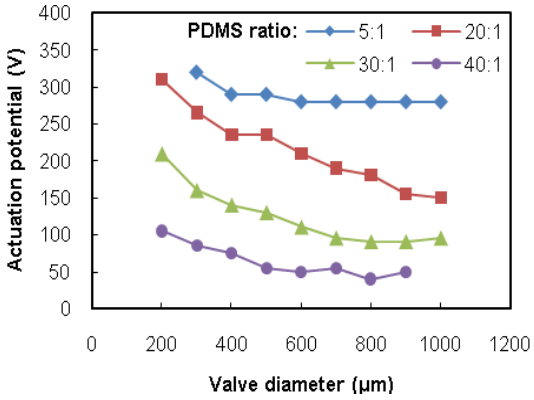

Figure 12: Actuation potentials for valves supported by solid slabs of PDMS with different monomer/curing-agent ratios.

Comparison of analytical predictions and experimental observations

We next varied the gaps between electrodes in the microvalves using the same arrays as before and compared results with analytical predictions. Figure 13 shows that preliminary results agreed well with the model. The differences between experimentally observed potentials and analytical could be due to inaccurate values of the material parameters used in the analytical predictions, such as Young's modulus and residual stress. Since the edge of the valve membrane was not clamped over the channel, the boundary conditions are different from those assumed in membrane stiffness expressions as well. Theoretical predictions are well within experimental uncertainties, however.

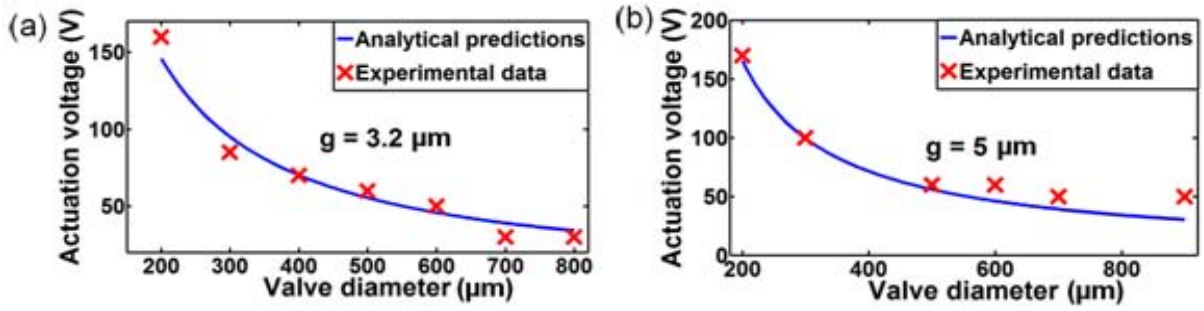

Figure 13: Comparisons between analytical predictions for actuation potential and experimental data.

When ITO/glass was used as the lower electrode, the valves remained closed due to strong surface adhesion forces (in agreement with equation 5). This was remedied by increasing the channel height, although doing so also increased the required actuation potential. The lowest observed actuation potential for a re-opening valve with an ITO/glass lower electrode was 200 V. However, our model suggests that modifying the surface properties of the lower electrode and optimizing parameters such as membrane thickness could result in significantly lower actuation potentials.

Actuation with fluids

To test actuation and isolation pressures with fluids, we used MWNT/PDMS as a lower electrode. Actuation potentials on the MWNT/PDMS electrode were similar to those on the ITO/glass electrode. With 2 μm tall channels, none of the valves re-opened, but again, increasing the channel height was able to remedy the problem. We observed that with the same parameters, valves on a MWNT/PDMS surface re-opened more easily than valves on an ITO/glass surface.

Figure 9d shows an image of the edge of the electrode where the MWNT film is located. Since PDMS is exposed at the surface of the MWNT/PDMS electrode, the lower electrode can

be permanently bonded to the upper electrode with oxygen plasma. This allowed us to infuse various fluids through the valves without the valves bursting. We first characterized valve isolation pressures with air. Figure 14 shows the pressure needed to re-open a 500 µm wide valve (2 µm tall channel) in relation to the applied potential. The valves are also able to close with applied pressures, though these pressures are lower than the isolation pressures.

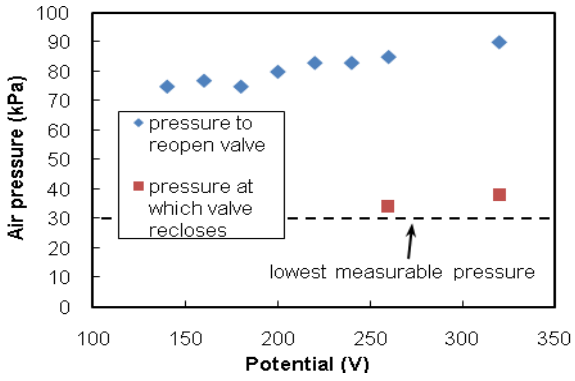

Figure 14: Isolation pressures for a 500 µm diameter microvalve.

We also tested the valves with a fluorinated oil (3M™ Fluorinert™ FC-40) and 18 MΩ water. Valves re-opened more easily when containing FC-40 as opposed to air, but isolation pressures were much lower. (We were unable to accurately measure the pressures with our current equipment). The lowest actuation potential for a valve which re-opened with the MWNT/PDMS lower electrode and containing FC-40 was 150 V.

With water, we were unable to completely close the valves which may have been due to dilute ions in the water that assemble at the electrodes when a potential is applied and screen the electric field. Others have circumvented this problem by using high frequency AC potentials,[8,9] and we are currently investigating the efficacy of these potentials with our system.

Actuate-to-Open Valve Geometry

Recent developments in microfluidic technology have led to the advancement of microfluidic valves formulated using multilayer soft lithography. One of the advances developed is the use of small microfluidic actuate-to-open valves. AtO valves are closed in rest and require the use of vacuum in order to open. They have previously demonstrated to be of value in high density reaction systems where multiples of reactions must be performed and then individually sealed off (Figure 15).[22]

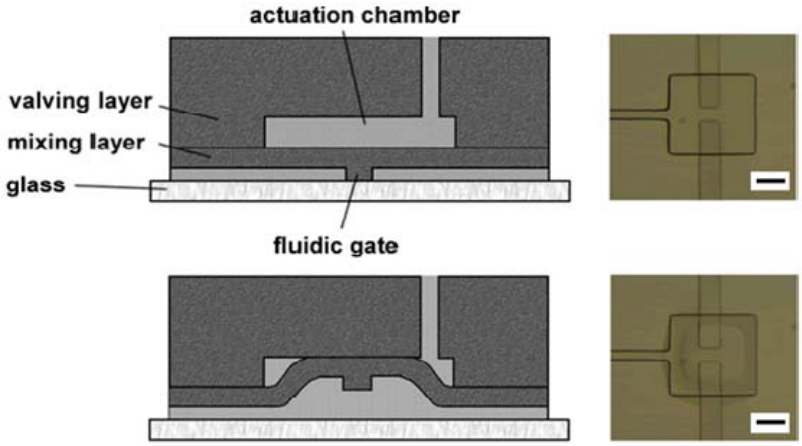

Figure 15: A schematic of Actuate-to-Open valves. When negative pressure is applied to the control layer microchannels, the thin PDMS layer beneath it will lift up, opening the chambers in between closed microchannels below (from ref 22). Scale bars represent 250 μm.

Further utilizing AtO valves in structures larger than the 4x4 system studied in the previous reference will require a greater understanding of valve operation and failure. For example, these valves have been observed to fail in operation, usually continuing to stick to the glass surface rather than open under vacuum. Factors such as valve geometry, asymmetry elements, and valve width have observed to be important in valve design, but have not been quantified to date.

The geometry of the valve at the point of initial opening was also expected to be an influential factor in the voltage or vacuum needed to open the closed valve. To this end, several designs of valve seat geometry (see Figure 16) were examined the effect of fluidic line geometry on the required pressure needed to open the valves. In a typical fabrication process, microfluidic channels in a control layer are aligned over microfluidic channels in a control layer. Altering this geometry in the fluidic channel is expected to introduce weak points, which should lower the required activation vacuum.

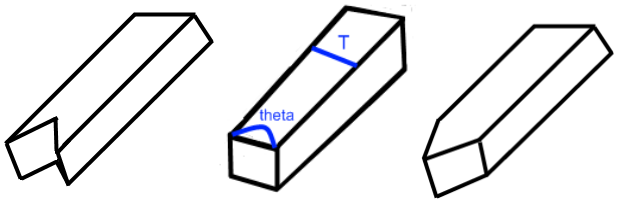

Figure 16: A schematic for the fluidic line geometries observed in this study. Each microfluidic channel terminated in an angle measured at 315^{o} (left), 180^{o} (center) and 90^{o} (right).

For each set of geometries, a series of microfluidic channels were fabricated using the technique referenced above. Each set of valves were hooked to a vacuum with a gauge line, with the pressure increased incrementally. The pressure difference required for each microchannel was then recorded when the valve opened (Figure 17).

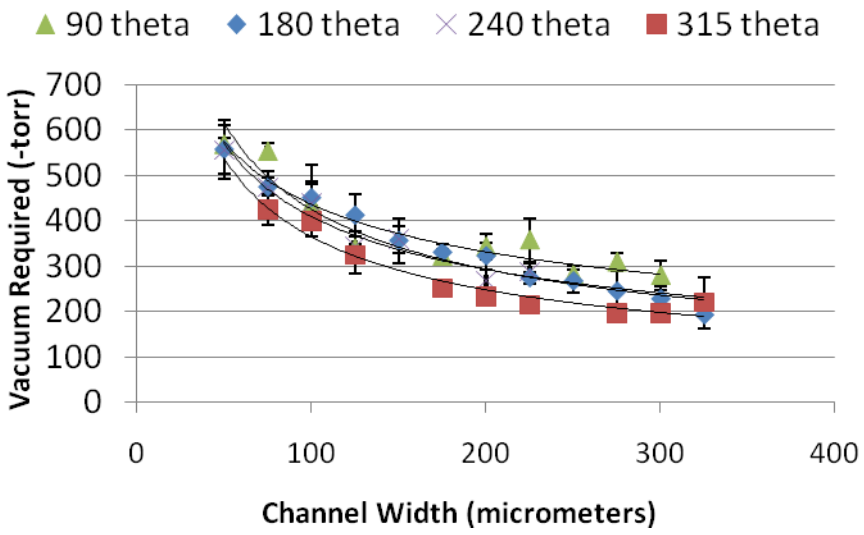

Figure 17: A graph of various devices being measured as a function of microfluidic channel width and geometrical termination. At the values we have studied, there is a slight dependence on terminal geometry, but not as strong as microchannel width.

Typically, the valves required less of a pressure difference as the width of the microchannel increased, which is expected due to pressure being an area-based force. As the width of the microchannels increase, the active area within the microchannel increases. Since area scales with pressure, the larger microchannels experience the same force as the smaller microchannels in order to open. The effect of geometry appears to be slight, with smaller angle termination being harder to open than large angle termination. It was expected that large angle terminations would effectively supply a lifting point for the valves to open, thereby reducing the vacuum required. However, it is possible that the microchannels designed for this project were too large for the terminated endpoint to have an effect. When the valves are groups by perimeter underneath the microchannel, the devices demonstrate a separation of data sets as evidenced by the graph in Figure 18.

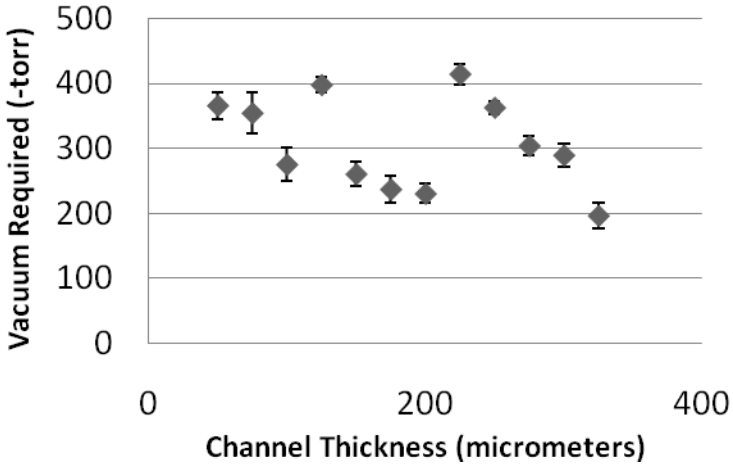

Figure 18: A graph of actuation points for a 90 degree terminated microfluidic channel.

One reason this trend does not follow previous data is due to a misalignment at points 125 um and 225+. Due to decreased perimeter for these devices, the microchannel actuation required higher vacuums.

Conclusions and Future Work

In summary, we created an analytical model that provided design rules applicable to the fabrication of elastomeric, electrostatic microvalves. After investigating several techniques for embedding conducting nanoparticles into an elastomeric membrane, we found that filtration followed by microtransfer printing was the most effective. We then incorporated the conducting membrane into arrays of electrostatic microvalves and found that actuation potentials correlated well with model predictions. Currently, valve design can be optimized to yield actuation potentials as low as 15 V.

Future work entails several main objectives. Firstly, design parameters need to be adjusted to produce microvalves that consistently open yet retain low actuation potentials. Secondly, the design of the microvalves needs to be modified so that it can accommodate the high-frequency

AC potentials needed to actuate in water. Currently, the resistance of the MWNT films used as electrodes is too high for this application, so we are investigating other conducting nanoparticles for suitability with our system (e.g. gold and silver nanoparticles). Finally, the electrostatic valve will be incorporated into an integrated microfluidic device to demonstrate fluid routing and pumping.

Appendices

Appendix A: Expression for static stiffness

The expression for static stiffness (k) of a square or circular membrane (two most common geometries for microfluidic valves) that is fixed or clamped along the outer edges under a uniformly distributed load is given by [18, 19]

$$k = K_{bilayer}\frac{K_{MS}}{K_{AR}}\left(K_{shape}^{1}\frac{E_{bm}t_m^{\,3}}{L_e^{\,4}}+K_{shape}^{2}\frac{\sigma_0\left(t_m+t_c\right)}{L_e^{\,2}}\right)$$

$$K_{bilayer}=1+\frac{E_c t_c^{\,3}\left(1-\nu_m^{\,2}\right)}{E_m t_m^{\,3}\left(1-\nu_c^{\,2}\right)}+\frac{3\left(1-\nu_m^{\,2}\right)\left(1+t_c/t_m\right)^2\left(1+E_m t_m/E_c t_c\right)}{\left(1+E_m t_m/E_c t_c\right)^2-\left(\nu_m+\nu_c E_m t_m/E_c t_c\right)^2}, \qquad \text{(A1)}$$

k: static stiffness of the membrane per unit area,

E_{bm}: biaxial modulus of the membrane and is given by $E_{bm}=E_m/1-\nu_m^{\,2}$,

E_m: Young's modulus of the membrane material,

ν_m: Poisson's ratio of the membrane material,

t_m: thickness of the membrane,

E_c: Young's modulus of the conducting material,

ν_c: Poisson's ratio of the conducting material,

t_c: thickness of the conducting layer,

σ_0: residual stress in the membrane,

L_e: equivalent planar dimension of the membrane (side length for a square membrane and diameter for a circular membrane),

K_{shape}^{1} and K_{shape}^{2}: shape factors that depend on whether the membrane is square or circular,

$K_{bilayer}$: factor to account for bilayer configuration, conducting layer over membrane,

K_{AR}: factor to account for aspect ratio (AR) and is given by $K_{AR} = 1 + (16/(1-\nu_m))(t_m / L_e)$,

K_{MS}: factor to account for membrane stresses (MS) and is given by $K_{MS} = 1 + 0.488(g/t_m)^2$.

Appendix B: Detailed fabrication procedure

Molds for fluid channels and support layer

Molds for microfluidic channels and the supporting layers of the devices were made from patterned photoresist on silicon. Masks were designed with Adobe® Illustrator® and printed onto film with a high resolution printer (5080 dpi) from University of Illinois printing services. Typically, negative photoresist was processed according to manufacturer specifications (SU8-5 and SU8-50 for fluid layers and support layers, respectively; Microchem Corp.) Features on the molds for the microfluidic channels were typically 1-10 μm tall, and features for the suport layers were 50 μm tall. After developing, the mold was treated with a vapor of (tridecafluoro-1,1,2,2-tetrahydro octyl)-1-trichlorosilane (United Chemical Technologies, Inc.) by placing the wafer in a vacuum desiccator for four hours with several drops of the silane. Note that the vacuum line passed through a column of solid NaOH to neutralize gaseous HCl resulting from the reaction.

Process for creating upper layers of microvalve

To create the upper portion of the electrostatic microvalve, a thin layer of PDMS (GE RTV 615, purchased through Hisco-Schaumburg) was first spin-coated onto the mold for microfluidic channels. Liquid PDMS precursors were dispensed in a ratio of 20:1 base/curing-agent by weight (20:1 PDMS), and after mixing, the PDMS was degassed in a vacuum desiccator for several minutes until no bubbles were visible. Liquid PDMS was spin-coated onto the mold for microfluidic channels at 7000 rpm for 60 s following a 10 s ramp. (This spin-rate represents a typical procedure. The spin-rate was modified as needed to create thinner or thicker layers of PDMS.) The thin PDMS layer was cured in an oven at 70°C for 30 min.

Next, a MWNT film was formed and patterned onto the first PDMS layer via microcontact printing. A stock solution MWNT was made in a ratio of 1 mg MWNT / 10 mg SDS / 1 mL 18 MΩ water. MWNT were >95 wt% purity, <1.5 wt% ash, and had 20-40 nm outer diameter and 10-30 μm length (Cheap Tubes Inc.). Both MWNT and SDS (Fisher Scientific) were used without further purification. The solution was placed in an ultrasonic bath for 30 min. and then centrifuged at 4000 rpm for 15 min. to remove unwanted aggregates. Between 1-3 mL of the MWNT solution was vacuum filtered through an alumina membrane filter with 0.2 μm pore size (Anopore inorganic membranes, Whatman). Following filtration, the resulting MWNT film was washed with EtOH or another alcohol until the filtrate was clear, colorless, and without bubbles. The film was allowed to dry for several minutes under ambient conditions, and then transferred with a PDMS stamp.

The stamp was made by pouring 20:1 PDMS over a silicon/photoresist mold and curing at 70°C for at least one hour, but usually overnight. To transfer the film, the stamp was brought into conformal contact with the MWNT film and slight pressure was applied by hand. When removed, the stamp picked up the selected areas of the MWNT film, and this MWNT pattern was aligned and set onto the previously formed PDMS layer. Again, pressure was applied by hand, and the stamp was peeled off the PDMS layer, leaving the MWNT film behind.

A homogeneous slurry of MWNT and 5:1 PDMS (~10 wt% MWNT) was made by repeatedly drawing the mixture over a surface with a razor blade. The slurry was then applied onto peripheral regions of the exposed MWNT film to serve as electrical contacts. The high concentration of curing-agent in the PDMS served to minimize curing time, which was ~5 min. at 70°C.

Next, a layer of 20:1 PDMS was spin-coated onto the MWNT film at 2400 rpm for 30 s with a 10 s ramp. This layer served both as an encapsulating layer and an adhesion layer for the support layer. To properly adhere to the support layer, the adhesion layer was heated at 70°C for 20-30 min. or until just slightly tacky. The support layer was formed by pouring liquid 5:1 PDMS over a mold and curing at 70°C for at least 15 min. (Longer cure times up to an hour also gave good results.) After, both layers were aligned and brought into conformal contact. If certain regions were misaligned, the layers could be de-sealed and then realigned without negative effects. Surplus vinyl groups in the adhesion layer reacted with surplus silicon hydrides in the support layer during the final cure of at least 60 min. at 70°C. During this cure, extra liquid PDMS was poured around the support layer and over the electrical contacts to fill in any gaps. The device was removed by cutting around the appropriate areas with a scalpel.

Process for creating lower electrode

The substrate used for creating the lower PDMS electrode was a polished silicon wafer treated with (tridecafluoro-1,1,2,2-tetrahydro octyl)-1-trichlorosilane in the same manner as the molds. A slurry of 20:1 PDMS and MWNT (~10 wt% MWNT) was mixed together with a razor blade and small amounts were dispensed on the silicon to serve as electrical contacts. A ~0.5 cm thick layer of 20:1 PDMS was poured onto the substrate and heated in an oven at 70°C for 20-30 min until the PDMS was slightly tacky. The slab of PDMS was cut out with a scalpel, and a MWNT film was microtransfer printed onto the underside (the side originally oriented against the silicon). Care was taken to insure that the MWNT film overlapped with the electrical contacts in the PDMS slab. The slab was then pressed down into the silicon substrate so that the MWNT film was directly against the silicon. When pressure was applied, the MWNT film appeared to turn darker, indicating that the PDMS slab was sufficiently sealed against the silicon surface.

The slab was fully cured by heating at 70°C for at least one hour without any applied pressure. When ready for use, the slab was simply peeled off the substrate.

Sealing upper electrode to lower electrode

To seal the upper electrode and lower electrode together permanently, both elements were treated with plasma and then aligned together. First, access holes were punched to the microfluidic channels with a sharpened needle. Both the upper and lower electrode were placed onto frosted glass slides and set in a plasma cleaner (Harrick Plasma, Extended model). The chamber was evacuated to 500 mTorr of atmospheric gases, and exposed to plasma under the "high" setting for 90 s. After exposure, the two halves were aligned, gently brought into contact, and then heated at least one hour at 70°C.

References

[1] V. Studer, G. Hang, A Pandolfi, M. Ortiz, S. Quake, *J. Apply. Phys.* **951** (2004) 393-398.
[2] D. Biegelsen, A. Berlin, P. Cheung, M. Fromherz, D. Goldberg, W. Jackson, B. Preas, J. Reich, L. Swartz, *Proc. SPIE*, **4174** (2000), 299-306.
[3] S. Hua, F. Sachs, D. Yang, H. D. Chopra, *Anal. Chem.* **74** (2002) 6392-6396.
[4] C. C. Lee, G. D. Sui, A. Elizarov, C. Y. J. Shu, Y. S. Shin, A. N. Dooley, J. Huang, A. Daridon, P. Wyatt, D. Stout, H. C. Kolb, O. N. Witte, N. Satyamurthy, J. R. Heath, M. E. Phelps, S. R. Quake and H. R. Tseng, *Science* **2005**, 310, 1793-1796.
[5] M. Diehn, R. W. Cho, N. A. Lobo, T. Kalisky, M. J. Dorie, A. N. Kulp, D. L. Qian, J. S. Lam, L. E. Ailles, M. Z. Wong, B. Joshua, M. J. Kaplan, I. Wapnir, F. M. Dirbas, G. Somlo, C. Garberoglio, B. Paz, J. Shen, S. K. Lau, S. R. Quake, J. M. Brown, I. L. Weissman and M. F. Clarke, *Nature* **2009**, 458, 780-U123.
[6] M. A. Unger, H. P. Chou, T. Thorsen, A. Scherer and S. R. Quake, *Science* **2000**, 288, 113-116.
[7] K. W. Oh and C. H. Ahn, Journal of Micromechanics and Microengineering **2006**, 16, R13-R39.
[8] T. Bansal, M. P. Chang and M. M. Maharbiz, *Lab on a Chip* **2007**, 7, 164-166.
[9] M. P. Chang and M. M. Maharbiz, *Lab on a Chip* **2009**, 9, 1274-1281.
[10] A. S. Rollier, B. Legrand, D. Collard and L. Buchaillot, *Journal of Micromechanics and Microengineering* **2006**, 16, 794-801.
[11] T. L. Sounart, T. A. Michalske and K. R. Zavadil, *Journal of Microelectromechanical Systems* **2005**, 14, 125-133.
[12] M. Maghribi, J. Hamilton, D. Polla, K. Rose, T. Wilson and P. Krulevitch, *2nd Annual International IEEE-EMB Special Topic Conference on Microtechnologies in Medicine & Biology*
[13] A. Thangawng, R. Ruoff, M. Swartz and M. Glucksberg, *Biomedical Microdevices* **2007**, 9, 587-595.
[14] C. H. Mastrangelo and C. H. Hsu, *Microelectromechanical Systems, Journal of* **1993**, 2, 33-43.
[15] W. van der Wijngaart, H. Ask, P. Enoksson and G. Stemme, *Sensors and Actuators A: Physical* **2002**, 100, 264-271.
[16] C. H. Hu, C. H. Liu, L. Z. Chen, Y. C. Peng and S. S. Fan, *Applied Physics Letters* **2008**, 93, 3.
[17] C. Liu, *Advanced Materials* **2007**, 19, 3783-3790.
[18] M. Kaempgen, G. S. Duesberg and S. Roth, *Applied Surface Science* **2005**, 252, 425-429.
[19] Z. C. Wu, Z. H. Chen, X. Du, J. M. Logan, J. Sippel, M. Nikolou, K. Kamaras, J. R. Reynolds, D. B. Tanner, A. F. Hebard and A. G. Rinzler, *Science* **2004**, 305, 1273-1276.
[20] Y. Zhou, L. Hu and G. Gruner, *Applied Physics Letters* **2006**, 88, 123109.
[21] M. A. Unger, H.-P. Chou, T. Thorsen, A. Scherer and S. R. Quake, Science, 2000, 288(5463), 113–116.
[22] Benjamin R. Schudel, Charles J. Choi, Brian T. Cunningham, Paul J. A. Kenis, Lab on a Chip, 2009, 9, 1676-1680.

DISTRIBUTION:

# of copies	MS	Name
3	1349	Christopher Apblett, 1815
1	1082	W. Kent Schubert, 1723
1	1349	Bill Hammetter, 1815
1	0888	Regan Stinnett, 1821
1	1082	Greg Ten Eyck, 1717
1	0899	Technical Library, 9536 (electronic copy)
1	0123	D. Chavez, 1011